JOURNAL OF MATERIALS SCIENCE 35 (2000) 1419–1425

Improvements in α-Fe_2O_3 ceramic sensors for reducing gases by addition of Sb_2O_3

ZHANG TIANSHU, P. HING
Advanced Materials Research Centre, Division of Materials Engineering, School of Applied Science, Nanyang Technological University, Nanyang Avenue, Singapore 639798

ZHANG RUIFANG
Department of Materials Science and Engineering, University of Science and Technology of China, Hefei, Anhui 230026, People's Republic of China
E-mail: P1247137@ntu.edu.sg

The microstructure, electrical properties and gas-sensing characteristics of Sb-doped α-Fe_2O_3 were investigated. Powder precursors with Sb/Fe = 0–0.1 were prepared by chemical coprecipitation method. Sb-doped α-Fe_2O_3 powders were characterized by means of thermal gravimetric-differential thermal analysis (TG-DTA), X-ray diffraction (XRD), BET surface area and scanning electron microscope (SEM). It was found that the raw powders underwent crystallization into the corundum structure of α-Fe_2O_3 at a temperature which increased somewhat with increasing Sb content; a proper amount of Sb doping suppressed both crystallite growth and the formation of hard agglomerates. The doping of Sb_2O_3 decreased the sensor resistance by one order of magnitude and increased the sensitivities to some hydrocarbon gases markedly. The former can be attributed to the substitution of Sb^{5+} for Fe^{3+} sites in α-Fe_2O_3 generating more free electrons; the latter is closely related to Sb-doped samples accommodating a higher density of chemisorbed oxygen. © *2000 Kluwer Academic Publishers*

1. Introduction

Both γ-Fe_2O_3 and α-Fe_2O_3 have been studied as gas-sensing materials [1–3]. Generally speaking, the single phase of γ-Fe_2O_3 shows much better sensitivities to reducing gases than that of pure γ-Fe_2O_3 due to a big difference in gas-sensing mechanism [4, 5]. The crystal structure of γ-Fe_2O_3 is the same spinel type as that of Fe_3O_4. These two compounds can form a solid solution as follows [5]:

$$Fe^{3+}\left[\square_{x/3}Fe^{2+}_{1-x}Fe^{3+}_{(3+2x)/3}\right]O_4$$

$\square$: cation vacancy x: degree of oxidation

$$(0 \leq x \leq 1) \quad (1)$$

When $x = 1$, it corresponds to γ-Fe_2O_3 having a high resistivity similar to that of α-Fe_2O_3; when $x = 0$, it corresponds to Fe_3O_4 having a very low resistivity. However, no solid solution can be formed between α-Fe_2O_3 (corundum type) and Fe_3O_4 because of their different crystal structure. When a γ-Fe_2O_3-based sensor is placed in a reducing gas atmosphere, it is very easier for Fe^{3+} to be reduced into Fe^{2+} on the surface of γ-Fe_2O_3 grains than those on the surface of α-Fe_2O_3. The gas-sensing mechanism of γ-Fe_2O_3 is due to an electron exchange process between Fe^{3+} and Fe^{2+} in the solid solution of γ-Fe_2O_3 and Fe_3O_4, which can be considered as a kind of bulk effect.

In contrast, the gas-sensing mechanism of α-Fe_2O_3, to a large extent, is similar to that of SnO_2 due to the surface conductivity changes caused by the catalytic oxidation of the reducing gases with the chemisorbed oxygen related species, such as O^- or O^{2-} [6, 7]. It is well known that α-Fe_2O_3 have a high chemical stability. However, its high resistivity and poor sensitivity are far from the practical uses as gas sensors. Some investigations showed that the gas sensitivities of α-Fe_2O_3 can be greatly enhanced by adding quadravalent Ti, Zr and Sn to it [8, 9] or by preparing it from a solution iron sulphate [10]. The main reasons are that those dopants, such as Ti^{4+}, Zr^{4+}, Sn^{4+} or SO_4^{2-} suppress the grain growth and crystallization and consequently increase the specific surface of α-Fe_2O_3-based sensors. In the meanwhile, thin-film gas sensor using α-Fe_2O_3 prepared by CVD or sputtering technique have been studied recently [11, 12]. The sensitivities to reducing gases can be further enhanced in the form of multilayers, which a thin layer composed of SnO_2, WO_3 or Pt was deposited on a α-Fe_2O_3 layer [13, 14]. However, it seems that the sensitivities were not up to those of its ceramic gas sensors.

Antimony oxides are often used as conductive dopants for oxide semiconductors. For example, the addition of Sb_2O_3 to SnO_2-based materials has been widely studied because of their potential use as transparent electrodes [15–18] and gas sensors [19–21]. The SnO_2-based sensors doped with the proper amount of Sb_2O_3 can greatly reduced the resistance but the sensitivities are also lowed [22]. During the practical use, it

is necessary to add a catalyst, such as Pt or Pd, to the sensors in order to improve their sensitivities.

In this study, we have found, however, that for the α-Fe_2O_3-based system, a decrease in resistance by one order of magnitude and a remarkable improvement in gas sensitivity can be obtained by adding Sb_2O_3. The effects of Sb_2O_3 doping on microstructure, electrical properties and sensitivities of α-Fe_2O_3 system are represented.

2. Experimental procedure

2.1. Preparation of powder precursors

A coprecipitation method was used for preparing Sb-doped α-Fe_2O_3 powder precursors. Analytically pure reagents (A. R.) of $FeCl_3 \cdot 6H_2O$ and $SbCl_3$ were dissolved in water to form an aqueous solution having an atomic ratio of antimony-to-iron (Sb/Fe) ranging from 0 to 0.1. By adding ammonia (A. R.) to the solution at pH = 7. Sb-doped α-Fe_2O_3 precursors were precipitated, which was then washed, filtrated, dried and ground. The raw powder of antimony oxides was also prepared under the same condition.

2.2. Characterization of powder samples

The powder precursors with Sb/Fe = 0, 0.03 and 0.1 were subjected to thermal gravimetric-differential thermal analysis (TG-DTA) with a heating rate of 10°C min^{-1} up to 550°C in air. The crystal structure of the samples calcined at 650°C for 5 h in air was analysed using X-ray diffraction (XRD). The mean crystallite sizes (R_X) were measured from XRD peaks at a scan rate of 1° min^{-1} based on the Scherrer's equation:

$$R_X = 0.9\lambda/(\beta \cos \vartheta) \quad (2)$$

where λ (1.5406 Å) is the wavelength of X-ray, ϑ is the diffraction angle, β is the true half-peak width. The specific surface area of powders was studied using BET method by nitrogen absorption. The mean particle sizes, R_B (nm), was calculated from surface area data obtained by five-point analysis, S_W (m^2/g), and the true density, ρ_T (g/cm^3):

$$R_B = 6000/(\rho_T S_W) \quad (3)$$

2.3. Fabrication and characterization of gas sensors

Sb-doped α-Fe_2O_3 powder precursors were calcined at 650°C for 5 h in air. Gas sensors were fabricated by a bulk technology with above powders in a conventional way [23] and then sintered at 600°C for 5 h in air. Gas sensor elements were heated at about 450°C for 240 h in air for stabilization. The morphology of the sensor's surface was observed by scanning electron microscopy (SEM). The electrical resistances of the sensors were measured in the way described eleswhere [24], to obtain the gas sensitivity (S) defined as the ratio (R_a/R_g), where R_a and R_g are the sensor resistance measured in air and in the presence of the test gas, respectively.

3. Results

Fig. 1 shows the TG-DTA curves of the powder precursors of Sb-doped α-Fe_2O_3. A change in weight occurs at 90 to 130°C due to the dehydration of the samples; this dehydration also shows up on DTA as an endothermic peak. The second peak on DTA is exothermic and having no counterpart on TG, and it is ascribed to the crystallization of the samples. It is seem that the crystallization temperature became higher with increasing Sb content.

XRD patterns of Sb-doped α-Fe_2O_3 powders heated at 650°C for 5 h are shown in Fig. 2. No antimony oxides were detected by X-ray diffraction in the Sb content ranging from 0 to 0.1. The samples have a corundum structure as α-Fe_2O_3. With an increase in Sb content

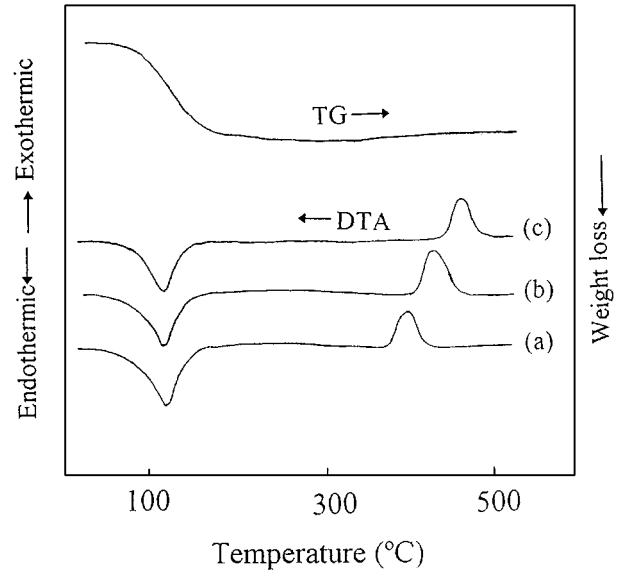

Figure 1 TG-DTA curves of α-Fe_2O_3 powders doped with and without Sb_2O_3: (a) Sb/Fe = 0; (b) Sb/Fe = 0.03; (c) Sb/Fe = 0.1.

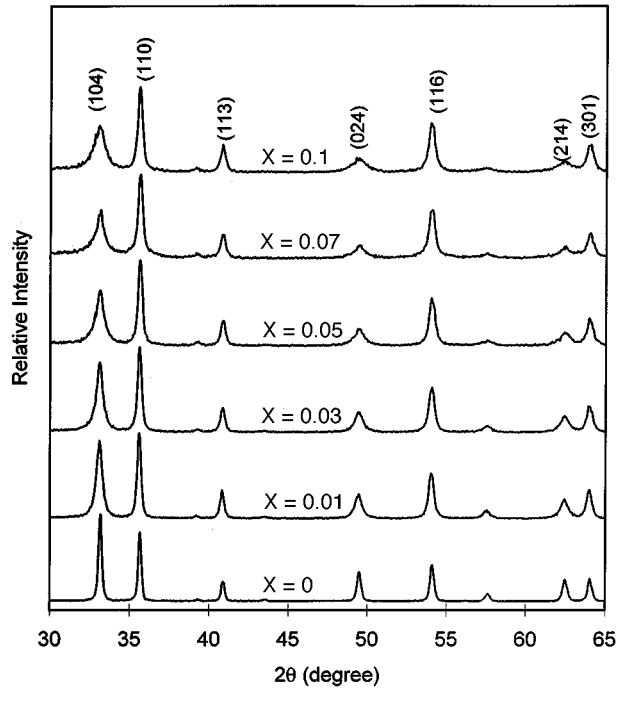

Figure 2 XRD patterns of Sb-doped α-Fe_2O_3 powders calcined at 650°C for 5 h. (X: molar ratio of Sb/Fe)

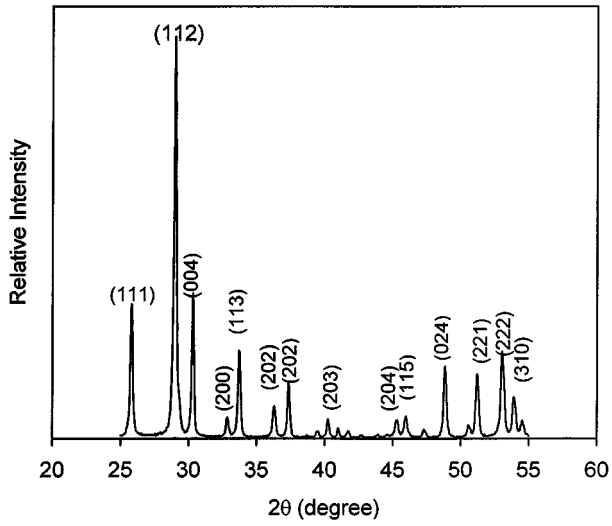

Figure 3 XRD pattern of antimony oxide precursor powder calcined at 650°C for 5 h.

doped XRD peaks become broader. On the other hand, it is observed that the Sb doping tended to promote the preferred orientation for (110), (116) and (301). In order to identify the phase of the antimony oxides in Sb-doped α-Fe_2O_3 powders, the raw powder of antimony oxides prepared under the same condition was calcined at 650°C for 5 h in air and analyzed by means of XRD. As shown in Fig. 3, the main phase is the compound of Sb_2O_4, which is the same as the study by Zaharescu *et al.* [25]. They found that when the calcination temperature is above 600°C, Sb_2O_3 can be oxidized into Sb_2O_4.

(104) and (110) XRD peaks as shown in Fig. 4 is used to obtain the mean crystallite sizes. With increasing Sb content, the height of the (104) peak becomes shorter and shorter, whereas (110) peak height has only a slight

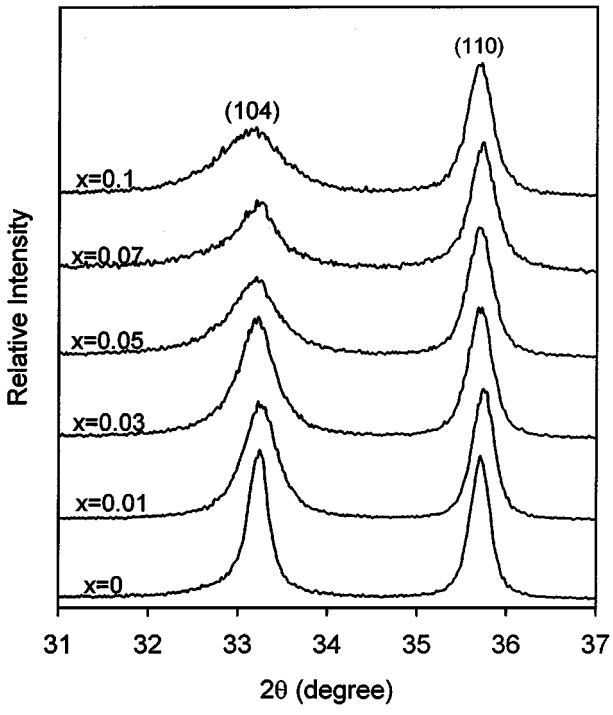

Figure 4 (104) and (110) XRD peaks used to estimate the crystallite sizes of Sb-doped α-Fe_2O_3 samples. (X: molar ratio of Sb/Fe)

TABLE I Effect of Sb content on crystallite sizes

Compositions (Sb/Fe molar ratio)	0	0.01	0.03	0.05	0.07	0.1
Crystallite sizes, R_X (nm) (after sintering)	27.2	18.5	16.4	15.7	14.8	13.2
Crystallite size, R_X (nm) (after thermal stabilisation)	37.3	21.1	17.7	16.6	15.4	13.5

TABLE II Properties of Sb-doped α-Fe_2O_3 powders

Compositions (Sb/Fe molar ratio)	0	0.01	0.03	0.05	0.07	0.1
BET surface, S_w (m^2/g) (after sintering)	37.1	52.3	68.8	82.3	98.8	106.8
BET surface, S_w (m^2/g) (after thermal stabilisation)	10.6	37.5	61.7	76.1	92.4	102.3
Particle size, R_B (nm) (after sintering)	60.0	45.2	32.3	27.3	22.5	20.8
Particle size, R_B (nm) (after thermal stabilisation)	210.5	64.0	38.1	31.0	26.3	22.8

change. The crystallite sizes from the former are small as Sb content increases compared to those from the latter. For example, based on the (104) or (110) peak, the crystallite sizes of the samples with Sb/Fe = 0, 0.03 and 0.1 were 26.4, 14.6 and 7.9 nm or 28.0, 19.7 and 18.6 nm, respectively. In order to reflect the true crystallite sizes, an average value was obtained from these two series and was listed in Table I. It is obvious that Sb doping can suppress crystallite growth of α-Fe_2O_3 during the sintering process. When the samples were heated at 450°C for 240 h, the crystallite sizes were calculated again and shown in Table I. The result indicates that for pure α-Fe_2O_3 there is a bigger increase in crystallite size, e.g., from 27.2 nm after sintering to 37.3 nm after thermal stabilisation. However, crystallite growth becomes slower and slower as Sb content increases.

On the other hand, when there are hard agglomerates in samples, the dimension of crystallites can not give the useful information for the gas-sensing materials. For this case, the specific surface area is a much more important parameter. In this study, the specific surface area was measured and the mean particle size, R_B, was estimated based on the Equation 3. The results were listed in Table II. For all the compositions the estimated particle size in Table II is bigger than the crystallite size in Table I, though when Sb/Fe $\geq$ 0.03, the value of the former goes near to that of the latter as shown in Table I and Table II. After thermal stabilisation, there is rapid increase in the mean particle size for pure α-Fe_2O_3, for example, from 60.0 to 210.5 nm after sintering and after thermal stabilisation, respectively. Referring to the change in the ratio of crystallite size after sintering and after thermal stabilisation (Table I), if would appear that very hard agglomerates must occur in the pure α-Fe_2O_3 powder because crystallite growth alone after thermal stabilisation can not lead to such a rapid decrease in the specific surface area. On the other hand, this kind of hard agglomerate becomes less pronounced in the Sb-doped α-Fe_2O_3 powders, especially for the samples with Sb/Fe $\geq$ 0.03.

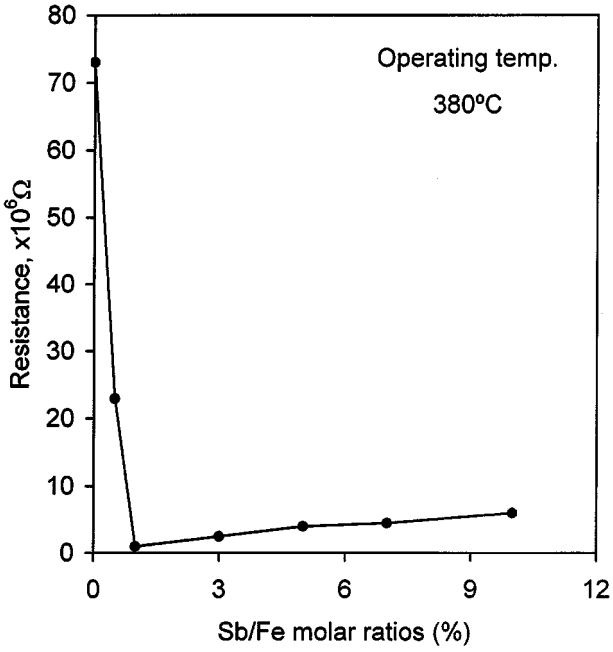

Figure 5 Relationship between Sb content and electrical resistance for sensor elements operating at 380°C.

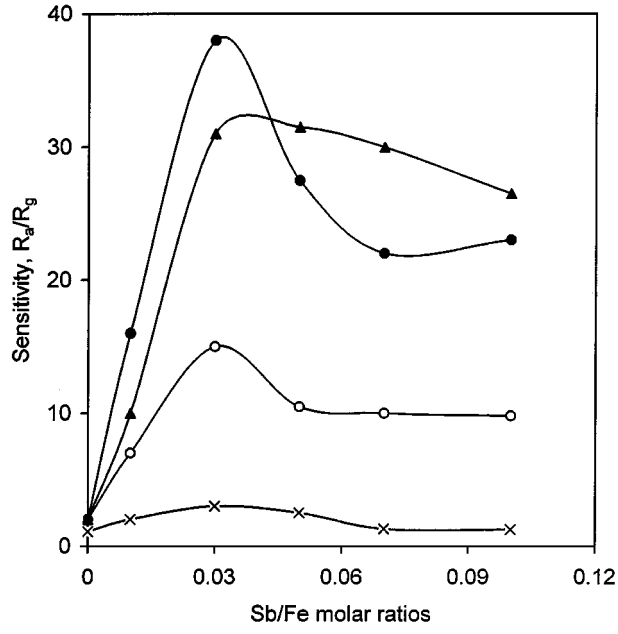

Figure 7 Effect of Sb content on the gas sensitivities of the sensors at 380°C: to gases (1000 ppm in air): ●: C_2H_2, ▲: Petrol, ○: LPG, ×: H_2 or CO.

The resistances of gas sensors in air at 380°C are shown as a function of Sb content in Fig. 5. In the region of Sb/Fe ≤ 0.01, the sensor resistance decreases steeply by over one order of magnitude with increasing Sb_2O_3, whereas in other region, it tends to increase slightly with the addition of Sb_2O_3.

As shown in Fig. 6, the Sb content obviously influenced on the conductance-temperature (σ-T) property of the sensors. In contrast to the monotonous σ-T curve of pure α-Fe_2O_3 based sensors (Fig. 6a), a plateau appears on the σ-T curves of Sb-doped α-Fe_2O_3-based sensors (Fig. 6b and c).

The gas sensitivities of sensors to several gases (1000 ppm in air) at 380°C are shown as a function of Sb content in Fig. 7. The pure α-Fe_2O_3 shows a very poor gas sensitivities. However, the Sb-doping up to about 0.03 increases the gas sensitivities to C_2H_2, petrol and LPG, while the sensitivity to H_2 or CO remains modest.

The sensitivities to reducing gases are greatly affected by operating temperature. As shown in Fig. 8, the sensor with Sb/Fe = 0.03 shows the highest sensitivities to the hydrocarbon gases, 1000 ppm in air each at 380°C, i.e., to C_2H_2, petrol and LPG, 38, 31 and 18 respectively. The sensitivity to 1000 ppm CO or 1000 ppm H_2 was only 4 at 380°C. The sensitivities to the hydrocarbon gases increase rather steeply with increasing gas concentration, without showing a saturating tendency up to 4000 ppm, as shown in Fig. 9. These results seem

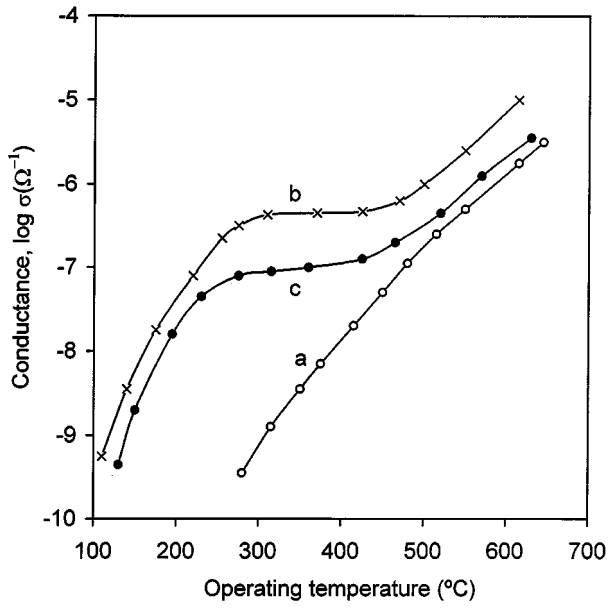

Figure 6 Conductance-temperature (σ-T) properties of sensors in air: (a): Sb/Fe = 0; (b): Sb/Fe = 0.03; (c): Sb/Fe = 0.1.

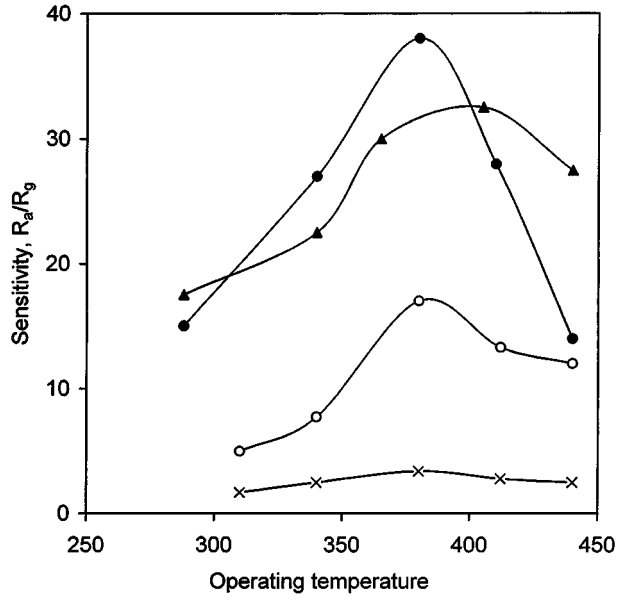

Figure 8 Effect of operating temperature on the gas sensitivities of the sensor (Sb/Fe = 0.03) to gases (1000 ppm in air): ●: C_2H_2, ▲: Petrol, ○: LPG, ×: H_2 or CO.

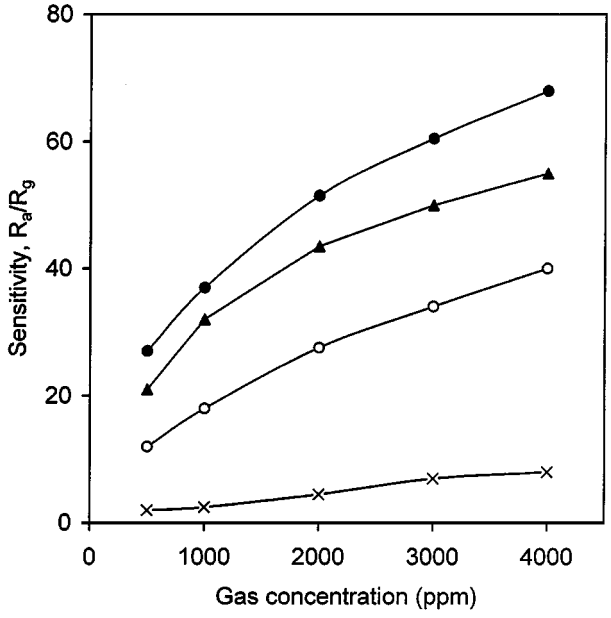

Figure 9 Gas sensitivity vs. gas concentration for the sensor (Sb/Fe = 0.03) at 380°C: ●: C_2H_2, ▲: Petrol, ○: LPG, ×: H_2 or CO.

to assure that Sb-doped α-Fe_2O_3 is suitable for sensing the hydrocarbon gases.

4. Discussion

4.1. Effect of Sb doping on conductance

The resistance decreases rapidly upon the addition of antimony oxides up to Sb/Fe ≤ 0.01. When the molar ratio of Sb/Fe is greater than 0.01, there is a slight increase in its resistance. This phenomenon may be explained by the controlled valence mechanism. Although no antimony oxides were detected by XRD in the samples with Sb/Fe = 0 to 0.1, based on our experiment result in Fig. 3 it is obvious that antimony oxides exist in the samples sintered at 650°C as the form of Sb_2O_4, a heterovalent mixture of Sb(III)Sb(V)O_4 [25] because the tetravalent state of antimony can't exist stably under the normal condition, i.e.:

$$Sb_2O_4 \Leftrightarrow Sb(III)Sb(V)O_4 \tag{4}$$

The antimony doping effect would then be different depending on Sb^{3+} or Sb^{5+} replaces Fe^{3+} sites. When one compares the relevant ionic radius ($Fe^{3+} = 0.64$ nm, $Sb^{5+} = 0.62$ nm and $Sb^{3+} = 0.92$ nm), it seems reasonable for Sb^{5+} to replace Fe^{3+} in α-Fe_2O_3 crystallites. Replacing Fe^{3+} by Sb^{3+} generates no charge carries and only when Fe^{3+} is replaced by Sb^{5+}, a decrease in resistance would result in as follows. If a fixed amount of Sb^{5+} ion ($[Sb^{5+}]_x$) incorporates into α-Fe_2O_3 crystallites, taking the neutral conditions into consideration the concentration of Fe^{3+} equal to $2[Sb^{5+}]_x$ should be reduced into Fe^{2+}. Using Kroger-Vink defect notations,

$$\left[Fe^{x}_{Fe}\right]_{2-3x}[Sb^{\cdot\cdot}_{Fe}]_x[Fe'_{Fe}]_{2x}O_{3-x} \tag{5}$$

$[Fe'_{Fe}]$ is a donor which can donate one electron, i.e.:

$$[Fe'_{Fe}] \Rightarrow \left[Fe^{x}_{Fe}\right] + e' \tag{6}$$

where $[Fe'_{Fe}]$ denotes an Fe^{2+} ion occupying an Fe^{3+} site, and $[Fe^{x}_{Fe}]$ denotes an Fe^{3+} occupying an Fe^{3+} site. However, based on the Equation 4, if a fixed amount of Sb^{5+} ion in the α-Fe_2O_3 lattice, what happens to the same amount of chemically bounded Sb^{3+}. It seems that there are two possibilities: 1) Sb^{3+} and Sb^{5+} enter into α-Fe_2O_3 crystal lattice at the same time. 2) Due to ionic radius of Sb^{5+} similar to that of Fe^{3+} it is preferable for Sb^{5+} to enter into α-Fe_2O_3 crystallite lattice at the beginning of doping. The same amount of Sb^{3+} may then be converted into Sb^{5+}. This conversion will be finished until the Sb^{5+} doping action stops. It is realised that Sb doping in the first case leads to a larger lattice parameters than that in the second case. We once calculated the lattice parameters of the samples in all compositions used. No obvious increase in lattice parameters was found. It suggests that only Sb^{5+} can enter into α-Fe_2O_3 lattice. However, it is thought that this replacement would take place up to only a small amount of Sb^{5+} (Sb/Fe ≤ 0.01) judging from the behaviour of sensor resistance in Fig. 5. The Sb component doped in excess would have reaggregated from α-Fe_2O_3, Since no antimony oxides could be detected by XRD (Fig. 2). The excessive antimony might have been dispersed as amorphous Sb_2O_4 on the surface of α-Fe_2O_3 crystallites.

4.2. Conductance-temperature characteristic

K. H. Kim *et al.* [26] pointed out that O_2 is absorbed on oxygen vacancy defect $V^{\cdot\cdot}_O$ on the surface of α-Fe_2O_3 based on the following reactions:

$$1/2O_2(g) + V^{\cdot\cdot}_O + e^- \Leftrightarrow O^- - V^{\cdot\cdot}_O \tag{7}$$

$$O^- - V^{\cdot\cdot}_O + e^- \Leftrightarrow O^{2-} - V^{\cdot\cdot}_O \tag{8}$$

Where $O^- - V^{\cdot\cdot}_O$ and $O^{2-} - V^{\cdot\cdot}_O$ are a singly or doubly ionized oxygen atom couple with a surface oxygen vacancy. Sb doping leads to increase the concentrations of free electrons as already discussed. At a fixed air ambience, therefore, there is a big density of chemisorbed oxygen on the surface of Sb-doped α-Fe_2O_3 according to the above reaction formulas (7) and (8). The effect of chemisorbed oxygen on conductance is possibly more remarkable for Sb-doped α-Fe_2O_3. Based on the report by Takata *et al.* [27], with increasing temperatures there seems to be reversible changes among oxygen gas, chemisorbed oxygen and lattice oxygen:

$$O_{2gas} \Leftrightarrow O^-_{2ad} \Leftrightarrow O^{2-}_{ad} \Leftrightarrow O^{2-}_{ad} \Leftrightarrow O^{2-}_{lat} \tag{9}$$

Where the subscripts gas, ad and lat mean the state of gas, adsorption and lattice, respectively. So the plateau on the σ-T curves in Fig. 6 may be attributed to such an electron transfer process.

4.3. Gas-sensing properties

α-Fe_2O_3 has a high chemical stability compared to γ-Fe_2O_3, and a good coherence to substrates, i.e., a

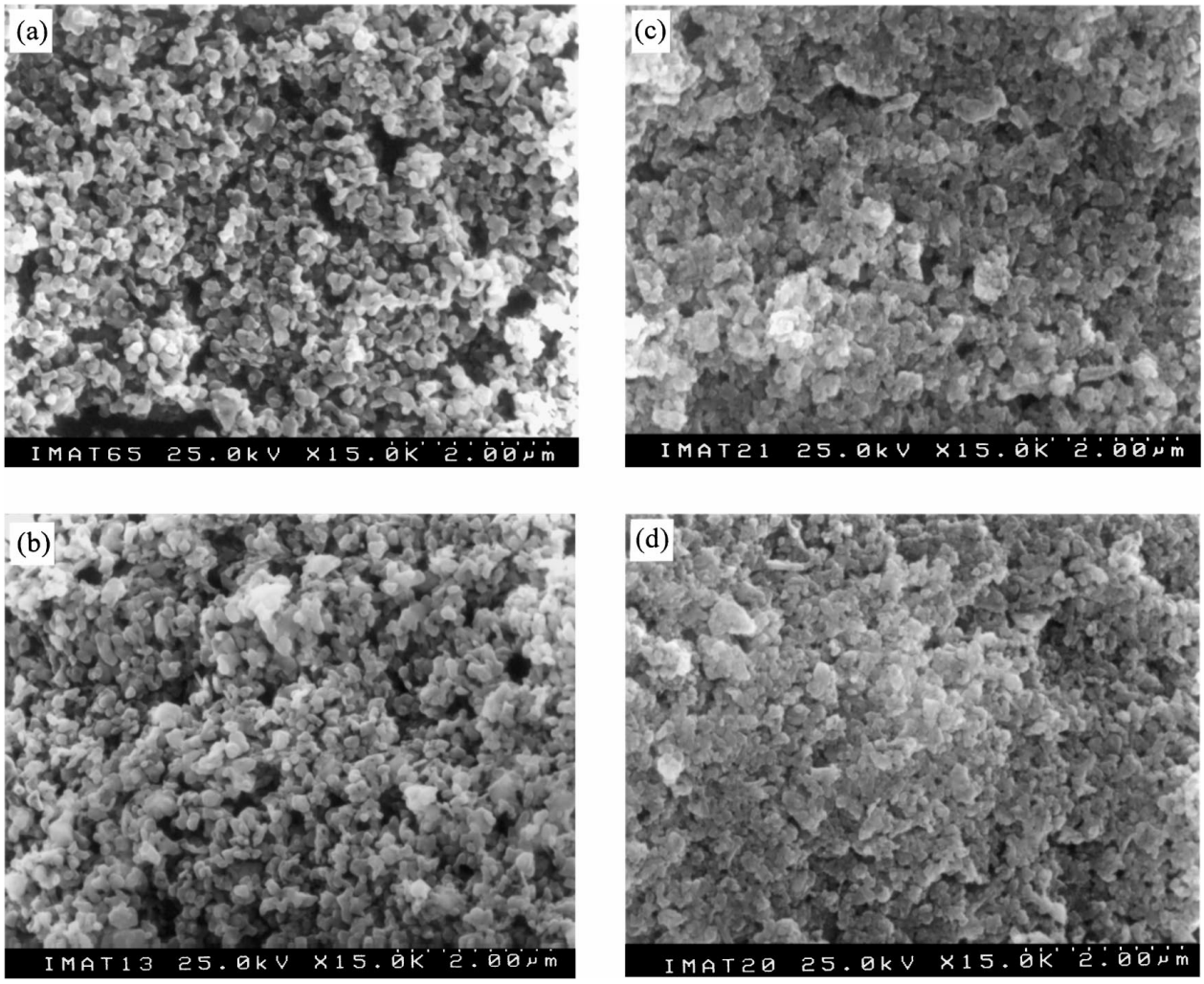

Figure 10 SEM photographs of the surface of sensors (Top view), before (a and c) and after (b and d) being heated at 450°C for 240 h in air: (a) and (b) pure α-Fe_2O_3; (c) and (d) Sb-doped α-Fe_2O_3 (Sb/Fe = 0.03).

sufficient mechanical strength, referred to SnO_2-based sensors. However, its too low sensitivity and too high resistivity restrict its practical use. Although so far some attempts have been done on α-Fe_2O_3 in order to improve these disadvantages, to our knowledge, no obvious improvement has been gotten yet. It is obvious that further work need to be done on the α-Fe_2O_3 system. The present work shows that Sb doping is an efficient method improving sensitivities of α-Fe_2O_3 based sensors.

The gas-sensing mechanism of α-Fe_2O_3-based sensors belongs to a surface-controlled model similar to that of SnO_2. In air there exists a steady-state density of electronic surface states related to oxygen species, such as O^-_{ad} and O^{2-}_{ad}, on α-Fe_2O_3-based sensors based on Equations 7 and 8. When a reducing gas (R) is introduced, an oxidation reaction will take place on the surface of sensor elements as follows:

$$O^- - V_O^{\cdot\cdot} + R \Rightarrow RO + V_O^{\cdot\cdot} + e^- \qquad (10)$$

and/or

$$O^{2-} - V_O^{\cdot\cdot} + R \Rightarrow RO + V_O^{\cdot\cdot} + 2e^- \qquad (11)$$

The increase of conductance arises from the above surface combustion process, which causes the return of electrons to α-Fe_2O_3 conduction band. It is obvious that the higher the density of chemisorded oxygen is, the better sensitivities of α-Fe_2O_3-based sensors are. So Sb doped α-Fe_2O_3-based sensors show a good sensitivity because a higher density of chemisorbed oxygen forms on their surfaces as mentioned above. Moreover, there may also be another reason. Before and after heated at 450°C for 240 h, as seen from Fig. 10, the sensor using Sb-doped powder (Sb/Fe = 0.03) kept almost the same surface morphology. In contrast, the one using pure α-Fe_2O_3 powder indicated after thermal stabilization, first, crystallite grains become bigger; secondly, there seems to be some kind of agglomeration into larger particles (Fig.10a and b) similar to the results from XRD and BET analyses. On the other hand, Sb doping suppresses both crystallite growth and the formation of hard agglomerates, thus may improve the long-term stability of α-Fe_2O_3-based sensors.

5. Conclusions

1) The Sb-doped α-Fe_2O_3 powders (with Sb/Fe = 0–0.1) prepared by chemical coprecipitation and calcination at 650°C for 5 h keep a corundum structure of α-Fe_2O_3. No other phases are detected.

2) Only a small amount of antimony (Sb/Fe $\leq$ 0.01) is considered to enter the lattice of α-Fe_2O_3. The rest

disperses as amorphous particles of Sb_2O_4 on α-Fe_2O_3 crystallites, which prevents the lattice ions of Fe^{3+} and O^{2-} from self-diffusing and avoids forming both big crystallites and hard agglomerates during the sintering process or operating condition. It may improve the long-term stability of Sb-doped α-Fe_2O_3-based sensors.

3) Sb-doped α-Fe_2O_3 leads to a decrease in sensor resistance by one order of magnitude and a remarkable improvement in sensitivities to some hydrocarbon gases such as C_2H_2, petrol and LPG. All the samples used, the sensor with $Sb/Fe = 0.03$ shows the highest sensitivities to the hydrocarbon gases and the sensitivities increase rapidly with increasing gas concentration, without showing a saturating tendency up to 4000 ppm.

References

1. W. CHUNG and D. LEE, *Thin Solid Films* **200** (1991) 329.
2. D. LEE and D. CHOI, *Sensors and Actuators* **B1** (1990) 231.
3. M. MATSUOKA, Y. NAKATANI and H. OHIDO, *Nat. Tech. Report* **24** (1978) 461.
4. C. CANTALINI, M. FACCIO, G. FERRI and PELINO, *Sensors and Actuators* **B18–19** (1994) 437.
5. Y. NAKATANI and M. MATSUOKA, *Jpn. J. Appl. Phys.* **22** (1983) 233.
6. K. D. SCHIERBAUM, V. WEIMAR and W. GOPEL, *Sensors and Actuators* **B3** (1991) 205 .
7. D. KOHL, *ibid.* **18** (1989) 71.
8. T. KOBAYASHI, M. HARUTA, H. SANO and M. NAKANE, *ibid.* **13** (1988) 339.
9. Y. NAKATANI, M. SAKAI and M. MATSUOKA, *Jpn. J. Appl. Phys.* **22** (1983) 912.
10. Y. NAKATANI and M. MATSUOKA, *ibid.* **21** (1982) L758.
11. K. HARA and N. NISHIDA, *Sensors and Actuators* **B20** (1994) 181.
12. J. PENG and C. C. CHAI, *ibid.* **B13–14** (1994) 591.
13. Y. DAHEI, M. XIAOCUI, W. ZONGCHANG and W. JUN, *Thin Solid Films* **224** (1993) 257.
14. K. HARA and N. HAYASHI, in Proc. 2nd Sensor Symp. Tsukuba, Japan, May 27–28, 1982, p. 209.
15. D. J. GOYAL, C. AGASHE, B. R. MARATHE, M. G. TAKWALE and V. G. BHIDE, *J. Appl. Phys.* **73** (1993) 7520.
16. T. H. KIM and K. H. YOON, *ibid.* **70** (1991) 2739.
17. K. H. KIM and S. W. LEE, *J. Am. Ceram. Soc.* **77** (1994) 915.
18. V. VASU and A. SUBRAHMANYAM, *Thin Solid Films* **202** (1991) 283.
19. M. IPPOMMATSU and H. SASAKI, *J. Electrochem. Soc.* **136** (1989) 2123.
20. Y. K. FANG and J. J. LEE, *Thin Solid Films* **169** (1989) 51.
21. A. M. AZAD, S. A. AKBAR, S. G. MHAISALKAR, L. D. BIRKEFELD and K. S. GOTO, *J. Electrochem. Soc.* **123** (1976) 199.
22. N. YAMAZOE, *Sensors and Actuators* **B5** (1991) 7.
23. K. TANAKA, S. MORIMOTO, S. SONODA, S. MATSUURA, K. MORIYA and M. EGASHIRA, *ibid.* **B3** (1991) 247.
24. S. S. V. COLES, K. J. GALLAGHER and J. WATSON, *ibid.* **7** (1985) 89.
25. M. ZAHARESCU, S. M. IHAIN, S. ZUCA and MATIASOVSKY, *J. Mater. Sci.* **26** (1991) 1666.
26. K. H. KIM, H. S. HAN and J. S. CHOI, *J. Phys. Chem.* **83** (1979) 1286.
27. M. TAKATA, D. TSUBONE and H. YANAGIDA, *J. Am. Ceram. Soc.* **59** (1976) 4.

Received 30 November 1998
and accepted 9 September 1999